Journal of Cleaner Production 237 (2019) 117793

Contents lists available at ScienceDirect

Journal of Cleaner Production

journal homepage: www.elsevier.com/locate/jclepro

Feasibility of incorporating phosphogypsum in ettringite-based binder from ladle slag☆

Katrijn Gijbels [a], Hoang Nguyen [b, *], Paivo Kinnunen [b], Wouter Schroeyers [a], Yiannis Pontikes [c], Sonja Schreurs [a], Mirja Illikainen [b]

[a] Hasselt University, CMK, Nuclear Technological Centre, Agoralaan, Gebouw H, 3590 Diepenbeek, Belgium
[b] Fibre and Particle Engineering Research Unit, University of Oulu, Pentti Kaiteran katu 1, 90014 Oulu, Finland
[c] KU Leuven, Department of Materials Engineering, Kasteelpark Arenberg 44, 3001 Leuven, Belgium

ARTICLE INFO

Article history:
Received 30 April 2019
Received in revised form
20 July 2019
Accepted 25 July 2019
Available online 26 July 2019

Handling editor: Jiri Jaromir Klemeš

Keywords:
Ladle slag
Phosphogypsum
Ettringite
Hydration
Mineralogy
Compressive strength

ABSTRACT

Aiming to utilize phosphogypsum (PG) as a construction material, this study investigated the potential use of PG as a calcium sulfate source for the production of an ettringite-based binder (LSG). Six compositions with different percentages and PG's of different origin were hydrated with ladle slag (LS) to form LSG. The hydration, mineralogy and compressive strength of all mixtures were investigated and compared with a reference LSG made of pure synthetic gypsum. The minor impurities in PG, the different particle size distribution as well as the mineralogy induced distinguishable effects on the heat of hydration, phase assemblage and morphology. The results showed that the use of side-stream PG instead of pure gypsum results in superior properties with a 60% increase in compressive strength. This investigation shows high potential to produce a completely by-product-based LSG by combining different sources of industrial side-streams with minimal chemical and energy use.

1. Introduction

Phosphogypsum (PG) is a residue of phosphate production with a very low recycling rate (less than 5%) (International Atomic Energy Agency (IAEA), 2013). Approximately 4–6 tonnes of PG are generated for each tonne of phosphoric acid produced (Rashad, 2017). Worldwide, this results in around 170 million tonnes per year of PG being disposed of. The total amount of PG in disposal sites is estimated to reach 7 to 8 billion tonnes by 2025 (International Atomic Energy Agency (IAEA), 2013). In addition, the world population is still increasing and hence food production will continue to grow, which requires an increase in phosphate fertilizer production. Therefore, there will be increasing levels of PG production and disposal, in most cases without purification (Rashad, 2017; Tayibi et al., 2009), which can cause serious environmental contamination due to impurities. This contamination may occur from radon gas, atmospheric contamination with fluoride, ground- and groundwater pollution with naturally occurring radionuclides, acidity, or mobile heavy metal anions (Cánovas et al., 2018). Therefore, the use of PG in construction materials would take advantage of the availability of this secondary resource and offer obvious environmental benefits.

Many obstacles hamper the utilization of PG as a construction material, however (Cánovas et al., 2018; Rashad, 2017), the main one being the presence of certain impurities. For example, the use of PG can lead to unwanted retarding effects on setting when mixed with ordinary or blended Portland cement (OPC) (Akin Altun and Sert, 2004; Rashad, 2017; Saadaoui et al., 2017). The incorporation of PG in OPC also caused a strength reduction (Smadi et al., 1999). PG may also contain enhanced concentrations of naturally occurring radionuclides (more specifically, the naturally occurring radium isotopes) (Cánovas et al., 2018), which limits its use for building applications (e.g. as gypsum board or in cement and concrete) (Council of the European Union, 2014). Therefore, disposal has remained the predominant fate for PG. Some studies

☆ The two first authors contributed equally to this research paper.

* Corresponding author.
E-mail addresses: katrijn.gijbels@uhasselt.be (K. Gijbels), hoang.nguyen@oulu.fi (H. Nguyen), paivo.kinnunen@oulu.fi (P. Kinnunen), wouter.schroeyers@uhasselt.be (W. Schroeyers), yiannis.pontikes@kuleuven.be (Y. Pontikes), sonja.schreurs@uhasselt.be (S. Schreurs), mirja.illikainen@oulu.fi (M. Illikainen).

https://doi.org/10.1016/j.jclepro.2019.117793

have suggested pre-treatment of PG such as calcinating, washing, and mechanical or chemical treatment (Al-Hwaiti, 2015; Hammas-Nasri et al., 2019; Koopman and Witkamp, 2002; Potgieter et al., 2003; Smadi et al., 1999). However, the economic feasibility of these treatments is questioned. Consequently, the possibility to use PG with minor or no treatment is of high interest.

An ettringite-based binder, a promising application-dependent alternative to OPC-based cementitious materials, can be formed by the reaction between Al-rich phases and calcium sulfate sources. The main crystalline phase of the binder is ettringite ($C_3A.3\bar{C}\bar{S}.32H$; refer to Table 1 for cement notation). The ettringite-based binder is reported to have many advantages in comparison to OPC: it can attain good mechanical properties (Kim et al., 2016; Nguyen et al., 2019a), high chemical resistance (Quillin, 2001), and the ability to stabilize heavy metals in its structure (Peysson et al., 2005). In a previous investigation (Nguyen et al., 2019a, 2019b), an ettringite-based binder (LSG) was produced from the hydration between ladle slag (LS, a by-product from the steel industry) and pure gypsum. The microstructure, mechanical properties and durability of the LSG were studied. In addition, a fiber-reinforced composite from LSG showed high mechanical performance with very low CO_2 emissions (Nguyen et al., 2019c) compared with other conventional high-performance OPC-based composites. LS can also react with water without the presence of calcium sulfate. However, these reaction products are metastable and their conversion leads to strength reduction at later ages (Nguyen et al., 2019a).

To utilize PG in a more efficient way, it is used as a calcium sulfate source in the present study to produce an ettringite-based binder. Since it consists of mainly $CaSO_4.2H_2O$ with some minor impurities, PG is able to replace pure gypsum partially or completely in the reaction with LS to form the LSG. The cementitious binder in this work is almost entirely a by-product-based binder with a minor content of citric acid as a retarder and, hence, is able to offer both environmental and economic benefits. However, for a better understanding of the feasibility of reusing PG in LSG, several aspects need to be studied: (1) the effects of impurities in PG on the fresh and hardened state of LSG; (2) the optimal dosage of PG that can be used in LSG to obtain good mechanical properties; and (3) the microstructure and phase characterization of the developed materials.

Encouraged by the prospect of better utilization of PG in the construction industry, and to fill the aforementioned research gaps, this experimental investigation aims to provide an understanding of the feasibility of using PG as a precursor for LSG. The effects of impurities from PG on the fresh and hardened state of LSG was studied. The former was investigated by monitoring the heat of hydration by isothermal calorimetry, while the latter was studied by assessing the compressive strength up to 3 months of curing. Additionally, the hydration and the reaction products were monitored using a range of complementary techniques such as X-ray diffraction (XRD), Fourier-transformed infrared (FTIR) spectroscopy and thermogravimetric analysis (TGA). Morphological analysis was performed with scanning electron microscopy (SEM). Six compositions with PG's of different origin are the subject of the present study, and they are compared with the LSG from pure gypsum developed in a previous study (Nguyen et al., 2019b). In conclusion, the optimized mixture and suggestions for the use of PG in LSG are proposed and discussed.

Table 1
Chemical composition (in wt%) of LS, G1, G2 and G3.

	LS	G1	G2	G3
CaO (C)	50.6	32.3	36.2	35.2
SiO_2 (S)	13.9	0.7	0.2	0.9
Al_2O_3 (A)	24.4	0.1	0.2	0.2
Fe_2O_3 (F)	0.4	0.1	–	–
SrO	–	–	0.6	–
MgO	3.8	0.4	0.2	–
SO_3 ($\bar{S}$)	0.4	42.0	40.5	50.3
TiO_2	4.1	–	–	–
CeO_2	–	–	0.2	–
P_2O_5	–	–	0.5	1.3
F^-	–	–	–	1.1
LOI at 950 °C	1.0	21.3	21.2	11.0
Others	1.4	3.1	0.2	–

2. Materials and methods

2.1. Materials

The LS was supplied by SSAB Europe Oy (Raahe, Finland). The slag was collected from the company's slag pit after cooling naturally. The free CaO content was found to be zero, measured according to EN 450−1 (European Committee for Standardization, 2012). The LS was ball milled (TPR-D-950-V-FU-EH, Germatec Germany) to reach a d_{50} value of 10 μm. The density of the LS was measured with a Quantachrome Multipycnometer (MPV-6DC) according to ASTM C204 (ASTM International, 2017) and was 3.0 g/cm^3. The Blaine value of the LS was determined according to EN 196−6 (European Committee for Standardization, 2010) and was 2640 ± 200 cm^2/g. As calcium sulfate sources, 3 types of gypsum were used in this study (hereafter referred to as G1, G2 and G3, respectively). The first type (G1) was synthetic gypsum ($CaSO_4.2H_2O$) supplied by VWR (product code 22451.360). The second type (G2) was PG derived from Yara Oy (Finland). The third type was a reference material (n° 434) collected from a PG processing plant in Gdansk (Poland), which was milled and homogenized by the International Atomic Energy Agency (IAEA) (Shakhashiro et al., 2011). G2 was dried at 60 °C in a laboratory oven for 24 h to remove all moisture. G1 and G3 were used as received. The particle size distribution of the LS, G1, G2 and G3 was determined by laser scattering (Beckman Coulter LS 13 320), using the Fraunhofer model (International Organization for Standardization (ISO), 2009). Isopropanol was used to avoid hydration during measurement. The chemical composition of the LS and G2 was analyzed by X-ray fluorescence analysis (XRF) using a Philips PW 1830 instrument. The matrix composition of G3 was provided by the IAEA and consisted of 96 wt% $CaSO_4.2H_2O$, 1−2 wt% P_2O_5, 1.2 wt % F^-, 1 wt% SiO_2 and 0.2 wt% Al_2O_3 (Shakhashiro et al., 2011). The chemical composition of all materials is summarized in Table 1.

XRD analysis (D2 PHASER, Bruker) was performed to investigate the mineralogy of LS, G1, G2 and G3. The X-ray tube was operated at 30 kV and 10 mA. Diffractograms were recorded in continuous PSD fast mode between 5° and 70° 2θ at 0.02° step width with a counting time of 0.3 s per step. As an internal standard, 10 wt% ZnO (99.9% purity, Merck) was added (Jansen et al., 2011; Madsen et al., 2011). The samples were prepared using the back loading technique and an anti-scatter slit was positioned 1 mm above the samples. During acquisition, the samples were rotated at 15 rpm. The obtained data were evaluated with EVA V.3.1 (Bruker AXS) software. For the quantitative analysis, MAUD (Lutterotti et al., 1999) was used based on the Rietveld method (Rietveld, 1969). The results were recalculated from the known ZnO content and are summarized in Table 2. During the time between sample preparation by the IAEA and the use of G3, part of the gypsum has been transformed into bassanite and anhydrite.

2.2. Sample preparation

A total of 7 paste samples (P0−P6) and 7 mortar samples (M0-M6) were prepared for investigation. The precursor was

Table 2
Mineralogy (in wt%) of LS, G1, G2 and G3.

	LS	G1	G2	G3
Calcio-olivine ($\gamma - C_2S$)	21.0	–	–	–
Tricalcium-aluminate (C_3A)	2.3	–	–	–
Mayenite ($C_{12}A_7$)	21.9	–	–	–
Periclase (MgO)	2.1	–	–	–
Perovskite ($CaTiO_3$)	1.3	–	–	–
Q-phase ($Ca_{20}Al_{26}Mg_3Si_3O_{68}$)	47.3	–	–	–
Gypsum ($C\bar{S}.2H$)	–	96.8	93.6	33.2
Bassanite ($C\bar{S}.0.5H$)	–	–	6.4	27.1
Anhydrite ($C\bar{S}$)	–	3.2	–	32.1
Amorphous	4.0	–	–	7.6

composed of variable contents of LS, G1, G2 and G3. The specific ratios for each sample are presented in Table 3. According to previous work (Nguyen et al., 2019a), the content of gypsum was set at 30 wt%. Citric acid, supplied by Tokyo Chemical Industry Co., Ltd., Japan (product code C1949), was used as a set retarder (Nguyen et al., 2019b). The solution displayed a concentration of 0.5% citric acid and was made by dissolving the solid in distilled water using magnetic stirring at a speed of 250 rpm for 30 min at room temperature. Based on previous work (Nguyen et al., 2019a, 2019b), the liquid-to-precursor ratio (L/P) was established at 0.45. For the preparation of the mortar samples, CEN standard sand (DIN EN 196−1) was used with a sand-to-precursor ratio (S/P) of 3 (European Committee for Standardization, 2016). Paste samples were prepared by mixing the precursor and gradually adding the solution, followed by manually mixing for 3 min to obtain good homogeneity. The mixing of mortar samples was performed in accordance with EN 196−6 (European Committee for Standardization, 2010). After mixing, fresh pastes were cast in silicon cubic molds of 35 mm × 35 mm × 35 mm, while mortars were cast in steel molds with dimensions 40 mm × 40 mm × 160 mm according to EN 196−6 (European Committee for Standardization, 2010). After casting, the molds were stored in sealed plastic bags to avoid the loss of water. After 24 h, paste and mortar samples were removed from the molds and were further cured under water at room temperature until testing.

3. Methods

In order to study the heat evolution during hydration, isothermal calorimetry was performed on fresh pastes using a TAM Air Calorimeter at a set temperature of 25 °C during the first 8 days of hydration. Paste samples were mixed ex-situ and poured into glass ampoules, which were then inserted into the calorimeter. The heat flow signal was recorded automatically every second during the period of measurement.

As for phase characterization, XRD data were collected from paste samples after 28 days of curing, using the same device, measurement set-up and analysis method as for the characterization of the raw materials (i.e., LS, G1, G2 and G3). After their curing period, paste samples were air-dried at room temperature whereafter they were manually milled in a porcelain mortar. Crystalline ZnO (purity 99.9%, Merck) was added to the samples as an internal standard by 10 wt%.

FTIR (Vertex 70, Bruker) was applied on paste samples after 28 days of curing to identify the bonding characteristics of the developed materials. Spectra were acquired in wavenumber ranges from 4000 cm^{-1} to 600 cm^{-1}, at a resolution of 4 cm^{-1} and with 32 scans per measurement, supported by Opus software. The spectra were collected in ATR (attenuated total reflection) mode, using a diamond/ZnSe crystal with single interaction (PIKE Technologies Inc.). Prior to measurement, a background spectrum was recorded. In addition, TGA (Precisa prepASH 129) was carried out on paste samples after 28 days of curing, by heating the samples from 25 °C to 1000 °C under N_2 atmosphere, with a heating rate of 5 °C/min. Sample preparation for FTIR and TGA was the same as for XRD.

Compressive strength tests on mortar samples were undertaken in triplicate after 7, 28 and 90 days of curing on a Zwick Z100 or a Dartec with a load cell of 100 or 400 kN, respectively. SEM (Zeiss Sigma) was used to observe the morphology of the fracture surface of mortar samples after 7 and 28 days of curing after compressive strength testing. SEM samples were coated with 70 nm Pt prior to the observation. Images were collected in secondary electron (SE) mode with 5 kV acceleration voltage and a working distance of about 5 mm.

Table 3
Precursor mixture ratios (in wt%)[a].

	LS	G1	G2	G3
P0, M0	70	30	0	0
P1, M1	70	20	10	0
P2, M2	70	10	20	0
P3, M3	70	0	30	0
P4, M4	70	20	0	10
P5, M5	70	10	0	20
P6, M6	70	0	0	30

[a] P0−P6 and M0-M6 refer to paste and mortar samples, respectively.

4. Results and discussion

4.1. Particle size distribution

The particle size distribution of the used materials is presented in Fig. 1; a unimodal distribution is the result in each case. LS was characterized by particle sizes ranging from 0.1 μm to 223 μm, while the range for G1 was narrower, i.e., from 0.2 μm to 66 μm. The particle size of the Finnish PG (G2) was significantly larger compared with the Polish PG (G3). G2 consisted of particles with sizes ranging from 0.1 μm to 324 μm, with most particles ranging from approximately 20 μm−200 μm. The particle size of G3 ranged from 0.2 μm to 24 μm, with the highest particle population in the range from 2 μm to 20 μm. These data indicate that the average particle size of G3 was almost 10 times lower than the average particle size of G2. The d_{50} value for LS, G1, G2 and G3 was 10 μm, 12 μm, 66 μm and 7 μm, respectively. Differences in particle size distribution can have a significant influence on the hydration kinetics and microstructural development, and consequently on the final properties of the material (Liu et al., 2016). The L/P was established at 0.45 for all samples, although a decline in paste workability was observed upon substituting G1 by G3 (P4−P6); the use of the coarser G2 (P1−P3) slightly enhanced the workability. A lower particle size distribution needs more water for a given flowability because its higher specific surface area increases the water-absorption capacity and the interparticle forces, while finer particles hydrate also faster than coarser ones (Jiao et al., 2017; Roussel et al., 2010; Wallevik, 2009). The choice to not additionally mill G2 was based on our intention to restrict the overall production cost and energy investment of a future full-scale application. However, in future studies it is worth investigating how simple pre-treatment methods (e.g. milling) affect the workability and mechanical properties of mixtures.

4.2. Heat of hydration via isothermal calorimetry

The heat release during the hydration of paste samples was monitored by isothermal calorimetry and is presented in Fig. 2. The

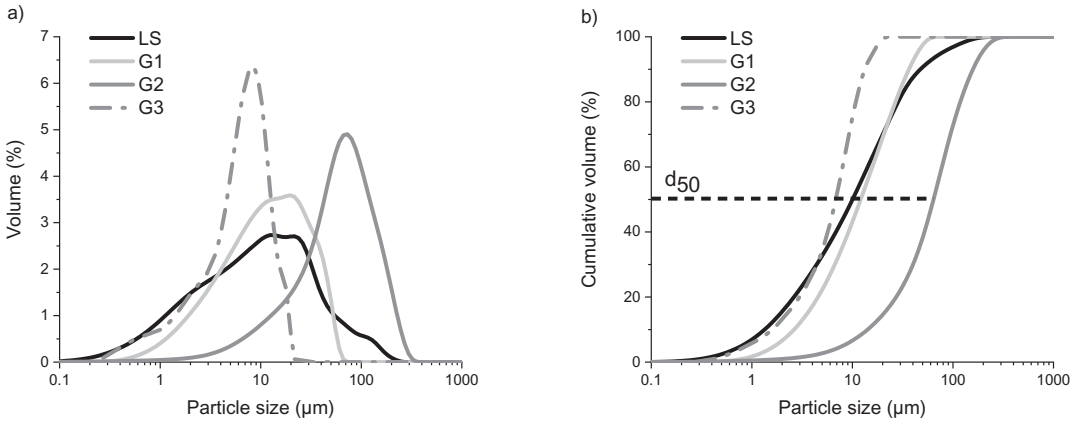

Fig. 1. Particle size distribution of LS, G1, G2 and G3: a) volume and b) cumulative volume.

reaction between LS and G1 (P0) is manifested by an initial wetting and dissolution peak, followed by a main hydration peak 8 h after the start of the measurement. This high-intensity peak is attributed to the formation of ettringite, followed by a shoulder at around 28 h designating (1) secondary ettringite formation (Nguyen et al., 2019a), (2) the conversion of ettringite to monosulfate (Kirchheim et al., 2018) and/or (3) the densification of the C–S–H phase. The intensity of the initial wetting and dissolution peak is comparable for all samples, irrespective of the gypsum source used. The gradual substitution of gypsum by Finnish PG (i.e., P1–P3) decreased the heat release for the main hydration peak. The reaction rate was not affected, however, as the timing of these main hydration peaks did not shift. When gypsum is substituted by Polish PG (i.e., P4–P6), the height of the main hydration peak decreases and this peak is shifted in time (i.e., it occurs at 11 h for P4, 7 h for P5 and 16 h for P6). Interestingly, a dormant period occurs between the main hydration peak and the shoulder. This period increases when Polish PG content is increased. This may be due to an increased level of impurities in the precursor when the proportion of PG increases (Huang et al., 2016). The shoulder peaks at 42, 60 and 180 h for P4, P5 and P6, respectively. Along with the presence of impurities in PG, the differences in particle size distribution may also contribute to the

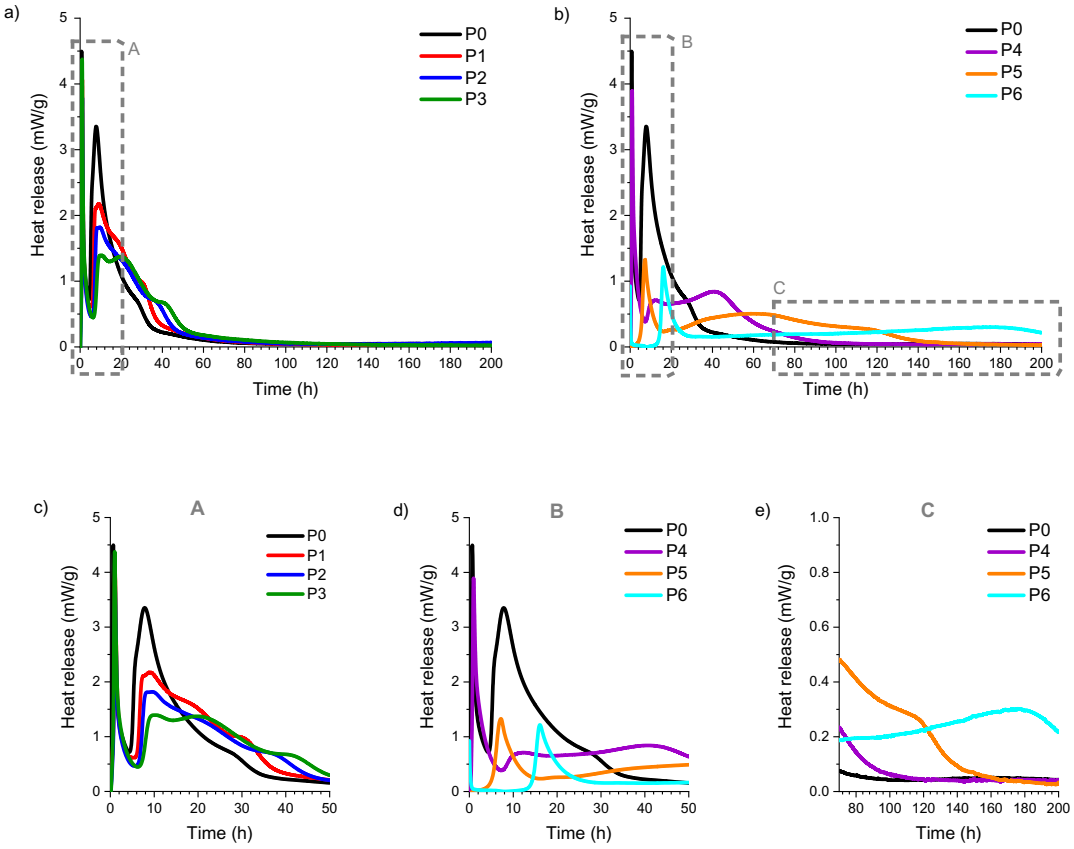

Fig. 2. Heat release of mixtures incorporating a) G2 (i.e., P1–P3), b) G3 (i.e., P4–P6) in comparison with the reference mixture P0, and the magnification of region c) A, d) B and e) C of the heat evolution.

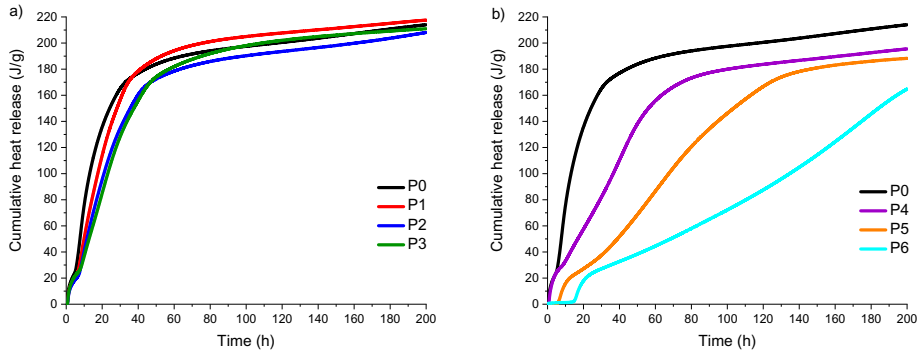

Fig. 3. Cumulative heat release of mixtures incorporating a) G2 (i.e., P1–P3) and b) G3 (i.e., P4–P6) in comparison with the reference mixture P0.

shifted heat evolution (Liu et al., 2016). In addition to $CaSO_4.2H_2O$, the Finnish PG also contains remnants of phosphoric acid, SrO and CeO_2. Phosphoric acid is known as a setting retarder for cement, as already extensively described in the literature ((Rashad, 2017) and references therein). However, the content of phosphoric acid in the Polish phosphogypsum (1–2 wt%) is almost 2 times higher compared with the Finnish PG (0.6 wt%). For this reason, the influence on the kinetics of the hydration reaction was greater for P4, P5 and P6, where the delay in reaction is directly proportional to the amount of gypsum substituted. In cementitious matrices, Sr^{2+} ions are immobilized due to the substitution of Ca^{2+} in the ettringite structure and by sorption on the C-(A)-S-H phase, while a small proportion of Sr^{2+} ions precipitates as $SrOH^{+}$ (Abdel Rahman et al., 2013). Ce^{3+} is expected to precipitate as insoluble CeO_2 or $Ce(OH)_3$ at alkaline pH, although incorporation into the ettringite and/or C-(A)-S-H phases may also be expected. F^{-} precipitates as insoluble CaF_2 in alkaline cementitious matrices (Park et al., 2008; Silveira et al., 2003) while it may also be incorporated in the ettringite phase or other mineral phases (e.g. fluorellestadite) (Gomes et al., 2012; He and Suito, 2008). The initial rapid precipitation of insoluble species such as $SrOH^{+}$, CeO_2, $Ce(OH)_3$ and CaF_2 is expected to decrease the heat release, by decreasing the available reactive surface of the precursor. Regarding P1, P2 and P3, it is likely that both (1) the presence of SrO, CeO_2 and phosphoric acid in G2 and (2) the higher particle size of G2 decreased the degree of reaction (i.e., the peak height). For P4, P5 and P6 both the decrease in the degree of reaction and the prolonged reaction rate may be due to the presence of F^{-} and phosphoric acid in G3, while it is also reasonable that both phenomena are being influenced by the small particle size of G3 (Liu et al., 2016), whereby a portion of the precursor gets covered by a rapid initial hydration product formation. It is also important to note that the sulfate sources showed variable mineralogy (i.e., a combination of gypsum, bassanite and/or anhydrite) which could also have influenced the hydration rate (Chandara et al., 2009; Pelletier-Chaignat et al., 2011). The rapid hydration of bassanite (for P4, P5 and P6) is not clearly distinguishable because the heat flow curves are the summation of heat released and consumed by various reactions that occur in sequence and/or in parallel during hydration. However, the notably prolonged shoulder for P4, P5 and P6 could be attributed to the slower anhydrite hydration. The kinetics of ettringite formation can influence its microstructural appearance, in which a fast reaction results in poorly-crystallized phases and a slower reaction results in a well-crystallized needle structure (Allevi et al., 2016).

The cumulative heat release is shown in Fig. 3. The use of PG's of different origin resulted in variable curve shapes. The gradual substitution of gypsum by Finnish PG (Fig. 3a) decreased the heat release during the first 40 h of hydration proportionally. Thereafter, the curves for P0, P1, P2 and P3 became quite similar, obtaining a cumulative heat of approximately 200 J/g after 200 h of hydration. From Fig. 3b it is clear that the substitution of gypsum by the Polish PG decreases and delays the heat release proportional to the substitution degree. The cumulative heat release after 200 h for P4, P5 and P6 is 195 J/g, 188 J/g and 164 J/g, respectively. From the slope of the curves it is concluded that the hydration of the pastes is still ongoing even after 200 h. The question remains to what extent the decreased and delayed reaction rate during the first 200 h has an influence on the final hydration products and properties of the material. This is investigated in the sections below.

4.3. X-ray diffraction

The X-ray diffractograms, obtained after 28 days of curing, are depicted in Fig. 4 from 5° to 40° 2θ. As already described in previous work (Nguyen et al., 2019a, 2019b), ettringite ($C_3A.3C\bar{S}.32H$) is the main crystalline phase produced upon the reaction between mayenite and gypsum (Eq. (1)), and tricalcium-aluminate and gypsum (Eq. (2)):

$$C_{12}A_7 + 12\ C\bar{S}.2H + 137\ H \rightarrow 4\ C_3A.3C\bar{S}.32H + 3\ AH_3 \quad (1)$$

$$C_3A + 3\ C\bar{S}.2H + 30\ H \rightarrow C_3A.3C\bar{S}.32H \quad (2)$$

Depending on the reactivity of the calcium sulfate source, the

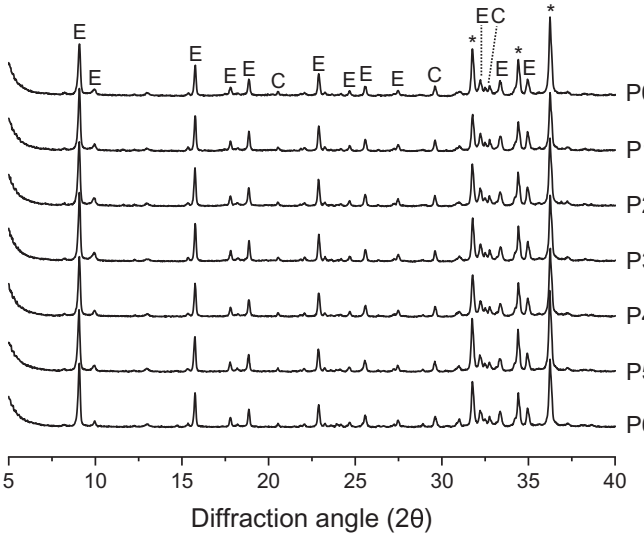

Fig. 4. XRD diffractograms of all paste mixtures after 28 days of curing.

water content, the depletion of calcium and sulfate by rapid ettringite formation and the pH, monosulfate ($C_4A\bar{S}H_{12}$) can be generated in sequence or in parallel from the hydration between mayenite and gypsum (Eq. (3)) and tricalcium-aluminate and gypsum (Eq. (4)), or from the conversion of ettringite to monosulfate (Eq. (5)) (Winnefeld and Lothenbach, 2010).

$$C_{12}A_7 + 4\,C\bar{S}.2H + 49\,H \rightarrow 4\,C_4A\bar{S}H_{12} + 3\,AH_3 \quad (3)$$

$$C_3A + C\bar{S}.2H + 10\,H \rightarrow C_4A\bar{S}H_{12} \quad (4)$$

$$C_3A.3C\bar{S}.32H \leftrightarrow C_4A\bar{S}H_{12} + 2\,C\bar{S}.2H + 16\,H \quad (5)$$

In most cases, however, monosulfate has a very low crystallinity and is therefore hard to detect by XRD (Gastaldi et al., 2016; Le Saout et al., 2004; Matschei et al., 2007). Aluminium-hydroxide (AH_3), a minor hydration product generated both in the reaction between mayenite and gypsum to form ettringite (Eq. (1)) and in the reaction between mayenite and gypsum to form monosulfate (Eq. (3)), is also ascribed to the amorphous part (Gastaldi et al., 2016; Qoku et al., 2017). The presence of Si from the calcio-olivine phase in the LS gives rise to amorphous C–S–H generation. Therefore, FTIR and TGA are useful complementary techniques to carry out in parallel with XRD. The aforementioned reactions (Eq. (1) - Eq. (5) and C–S–H generation) are expected to be the main hydration reactions, although this list is not exhaustive, e.g. minor hydration products linked to impurities such as fluoride (Jun et al., 2001; Pajares et al., 2002) and phosphorus (Huang et al., 2016) can also be formed. From Fig. 4, the main crystalline phases recognized are ettringite ("E") and calcio-olivine ("C"). The peaks of zincite are indicated with an asterisk.

Quantification of the amorphous and crystalline phases was performed using the Rietveld method (Rietveld, 1969) and is presented in Fig. 5a. The highest amorphous content was found for P0 (71.8 wt%), which decreased upon the substitution of G1 by G2 and G3. The ettringite content was comparable for all samples and ranged from 17.9 to 22.4 wt%. Small amounts of braunite (0.3–2.0 wt%) and jasmundite (<0.5 wt%) were identified as crystalline hydration products. In Fig. 5b, only the phases originating from the precursor are presented. The dissolution grade of the LS was significantly lower when PG was used instead of G1, likely due to the impurities from PG. For P0, neither gypsum, bassanite nor anhydrite were detected. For P1–P3, small amounts of gypsum (0.1–0.3 wt%), bassanite (0.4–0.6 wt%) and anhydrite (<0.3 wt%) were identified. For P4–P6, only bassanite (<0.4 wt%) and anhydrite (0.3–0.5 wt%) were discovered. It has to be noted here that the gypsum in P1–P3 may also be (partly) secondary gypsum, generated according to Eq. (5).

4.4. Fourier-transform infrared spectroscopy

FTIR spectra were recorded from paste samples after 28 days of curing. Curves are shown in Fig. 6. The bands noted at 3630 cm^{-1}, 3400 cm^{-1} and 1660 cm^{-1} are assigned to crystalline-bound water. The C–O bonding is deduced from the bands at 1400 cm^{-1} and 850 cm^{-1}. The Al–O–H bonding is recognized from the band at around 960 cm^{-1} and the S–O stretching occurs at 1100 cm^{-1} (Scholtzová et al., 2015). Whether or not these bands are induced by ettringite, monosulfate or aluminium-hydroxide is uncertain. However, in each case the intensity of these bands is higher for P0 and decreases upon substituting gypsum by PG, which could imply that fewer species were available for hydration product formation. This hypothesis would agree with Q-XRD in Fig. 5. Since the bands typical for Si–O bonding are overlapping, no firm conclusions can be drawn for the C–S–H phase. The bands from the C–O bonding could be related to (1) carbonation that has occurred during drying and milling of the pastes, and/or (2) the presence of thaumasite next to ettringite. However, carbonation was not observed in XRD, so it has occurred during sample preparation. Nevertheless, it was reduced when PG was used. From Fig. 6c, it is concluded that the spectra for P3 and P6 are generally quite similar (consistent with Q-XRD in Fig. 5), while the presence of the C–O bonding is lowest when the Polish PG was used (P6).

4.5. Thermogravimetric analysis

The graphs of TGA and the derivative thermogravimetric (DTG) curves are presented in Fig. 7. From the endothermic peak around 110 °C, the existence of the amorphous C–S–H phase is detected (Trauchessec et al., 2015). The largest endothermic peak from 150 to 180 °C is assigned to the decomposition of ettringite (Gaviria et al., 2018). The existence of monosulfate and aluminium-hydroxide can be deduced from the peaks located at around 180–200 °C and 200–300 °C, respectively (Qoku et al., 2017). The presence of gypsum (and bassanite) can be deduced from the region between 90 and 140 °C (Chang et al., 1999; Lou et al., 2011; Yu and Brouwers, 2012). Less aluminium-hydroxide was generated when the Polish

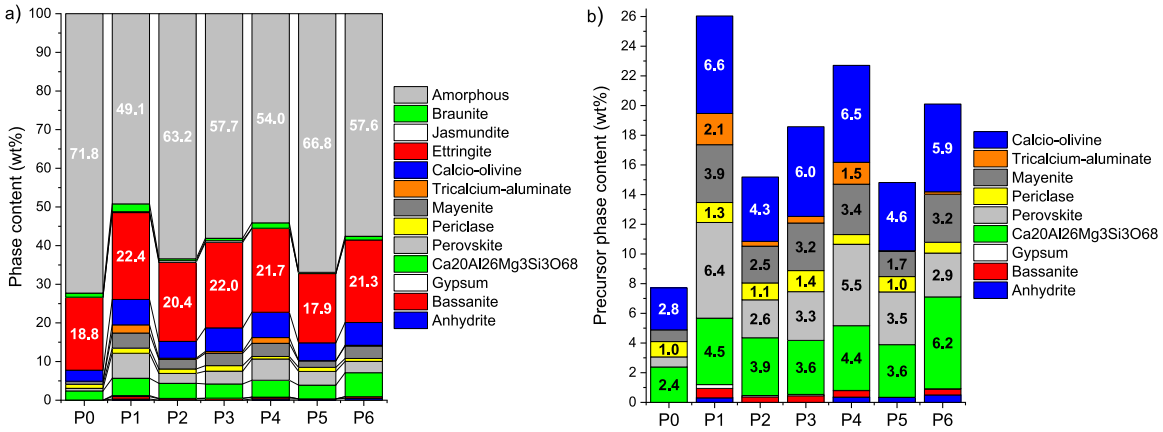

Fig. 5. Q-XRD after 28 days of curing: a) phase content of all paste mixtures and b) the content of leftover phases from the precursor (i.e., LS and (phospho-)gypsum) in these mixtures.

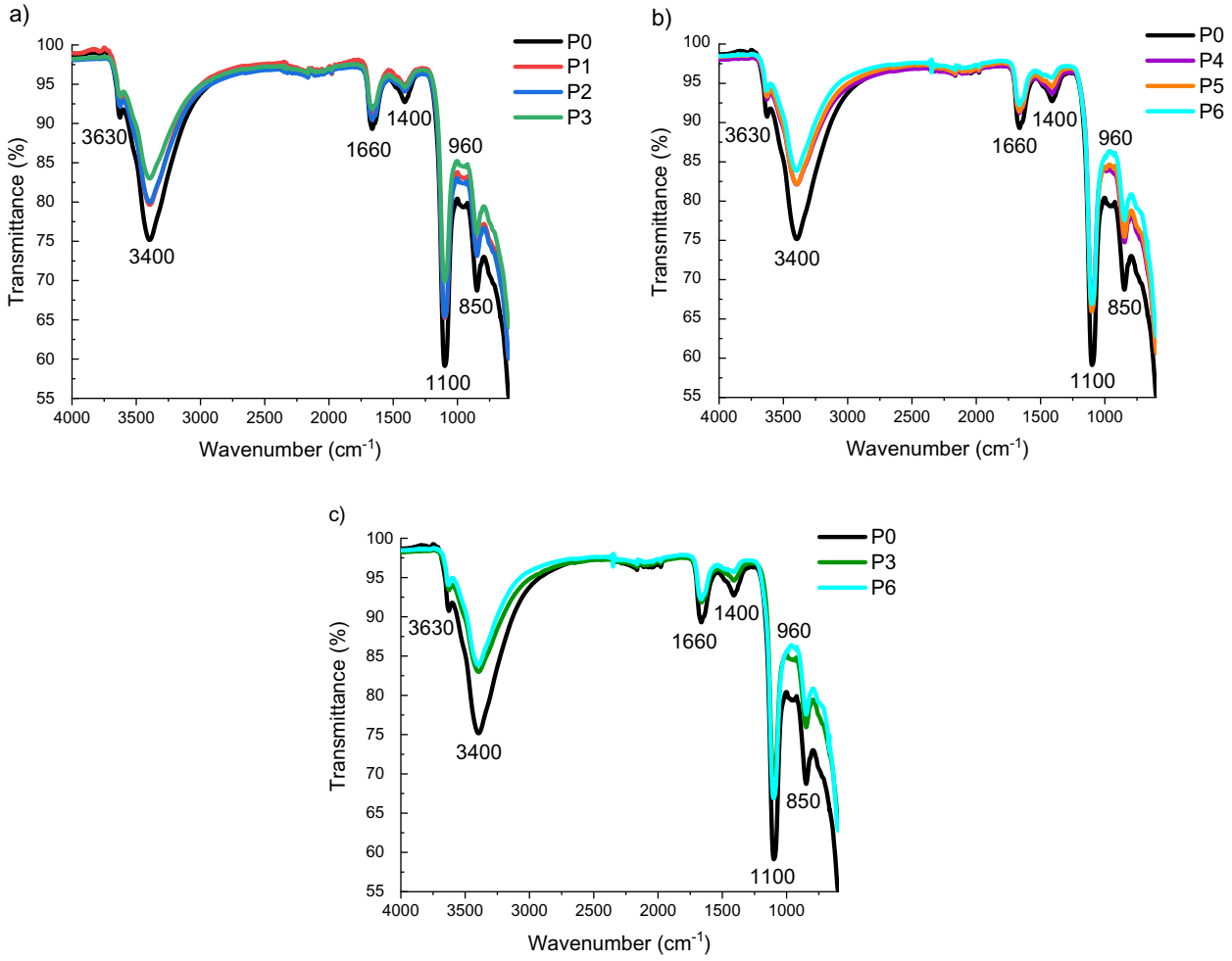

Fig. 6. FTIR spectra of mixtures incorporating a) G2 (i.e., P1–P3), b) G3 (i.e., P4–P6) in comparison with the reference mixture P0, and c) the comparison among P0, P3 and P6.

PG was incorporated (P4–P6), compared with P0. This means that (1) the formation of ettringite by Eq. (2) was more dominant than that by Eq. (1) and/or (2) the aluminium-hydroxide gets incorporated into the C–S–H gel resulting in a calcium-aluminosilicate-hydrate (C-A-S-H) phase. Both phenomena could result from slower kinetics compared with P0 (see Fig. 3b). From Fig. 7c it is concluded that the use of Finnish PG increases the monosulfate content compared with P0 (gypsum) and P6 (Polish PG). Since the aluminium-hydroxide content is not affected by the substitution of gypsum by Finnish PG (P1–P3), it is expected that the monosulfate generation is mainly carried out by Eq. (4) and Eq. (5). Consequently, it is possible that the formation of secondary gypsum by Eq. (5) (consistent with Q-XRD), together with remnants of bassanite have a cumulative effect on the region from 90 to 140 °C (and thus the C–S–H peak). After 28 days of curing, P3 contained 0.1 wt% gypsum and 0.4 wt% bassanite; P6 contained no gypsum and 0.4 wt % bassanite.

For P3, due to (1) secondary gypsum, (2) remnants of bassanite, (3) comparable ettringite and aluminium-hydroxide content and (4) an increased monosulfate content, the C-(A)-S-H content is lower compared with P0. For P6, it is expected that due to (1) unreacted bassanite, (2) comparable ettringite and monosulfate content and (3) a decreased aluminium-hydroxide content, the C-(A)-S-H content is equal or even slightly increased compared with P0. These expected changes in the amorphous phases are depicted in Fig. 8; the total amorphous content is derived from Q-XRD.

4.6. Compressive strength

In Fig. 9, the compressive strength after 7, 28 and 90 days of curing is presented. Upon the substitution of gypsum by Finnish PG (i.e., G2), the compressive strength is lowered and this reduction is in proportion to the amount of PG incorporated. In addition, mixtures with G2 developed full compressive strength after 7 days of curing, with negligible strength development in the period from 7 to 90 days of curing. This result is in good agreement with other ettringite-based binders reported as high early-age strength binders (Kim et al., 2016; Quillin, 2001). In contrast, the substitution of gypsum by the Polish PG (i.e., G3) increases the compressive strength considerably in the long term. Under the effects of impurities in G3, the strength development was delayed. The mortar samples attained their final strength after 28 days of curing, while there was no significant change in the compressive strength of these mortars when comparing the results after 28 and 90 days of curing. It is worth noting that, despite the delayed heat evolution of P5 (compared with P0) (Fig. 3b), M5 showed increased compressive strength (compared with M0) even after 7 days of curing. This is presumed to be a consequence of a better particle packing due to the smaller particle size of G3. In contradiction to the negative effects of impurities from PG on the strength of cementitious binders reported in (Akin Altun and Sert, 2004; Shen et al., 2014; Smadi et al., 1999), the use of G3 in LSG offered an increase of up to 60% in compressive strength. This is likely due to the late reactions, the

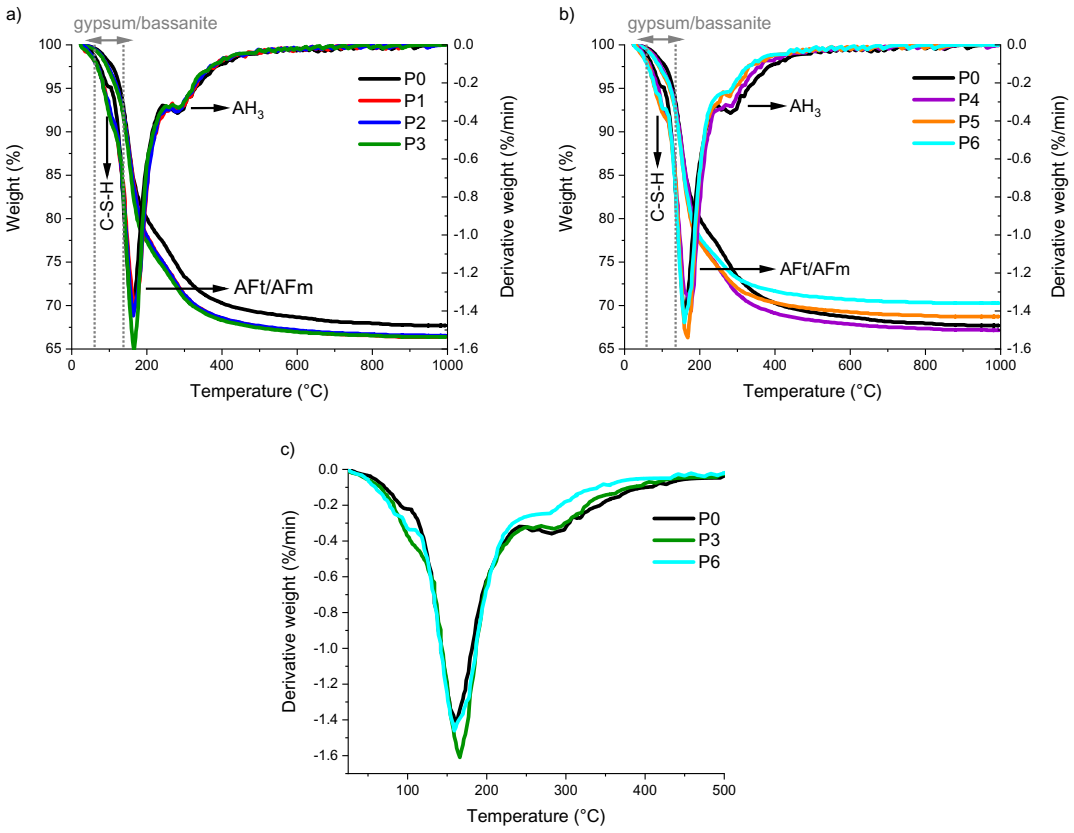

Fig. 7. TGA and DTG curves of mixtures incorporating a) G2 (i.e., P1–P3), b) G3 (i.e., P4–P6) in comparison with the reference mixture P0, and c) the comparison among P0, P3 and P6.

fine particle size of G3, which led to a denser LSG matrix, and changes in the crystalline and amorphous phase composition, as shown in Figs. 5 and 8, respectively. In addition, nitrogen adsorption/desorption tests were carried out in a parallel paper (Gijbels et al., 2019).

4.7. Morphological analysis

The fracture surface (after compressive strength testing) of mortar samples was investigated by SEM after 7 and 28 days of curing. Fig. 10 shows the SEM images of M3 and M6 after 28 days of curing, which represent the worst and the best combination in terms of compressive strength. It is clear that the main phase is ettringite (indicated as AFt in Fig. 10) for all mixtures from the reaction between LS and PG (Eqs. (1) and (2)). The phase was embedded in an amorphous matrix intermixed with undissolved LS particles and sand (indicated as FS in Fig. 10). In addition, the monosulfate phase (indicated as AFm in Fig. 10) has a layered structure consisting of positively charged layers balanced by water and anions in the interlayer (Baquerizo et al., 2015). As reported in e.g. (Gastaldi et al., 2016; Le Saout et al., 2004; Matschei et al., 2007), monosulfate is also a semi-ordered structure and hence can stay in the amorphous phase along with aluminium-hydroxide and C-(A)-S-H. Consequently, there was no monosulfate detected in the diffractograms shown in Fig. 4. Furthermore, the morphology of M6 exhibited a denser structure than that of M3 leading to higher compressive strength, which is likely due to a better particle packing and more pronounced hydration at a later age.

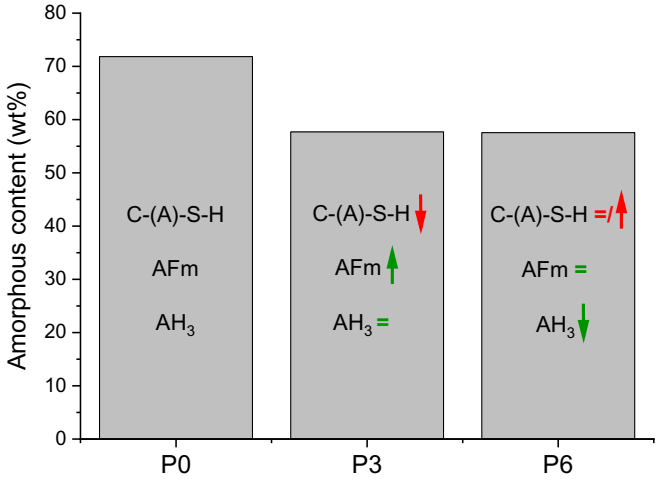

Fig. 8. Expectations of amorphous phase changes (in green, what is known; in red, what is expected).

5. Conclusions

This study investigated the potential use of Finnish (G2) and Polish PG (G3) as a potential calcium sulfate source for the production of LSGs. The results were compared with a reference LSG from pure gypsum (G1). During the first hours of hydration, the heat flow was decreased and delayed upon using PG, and these effects were more pronounced when using Polish PG. After 28 days of curing, the main crystalline phase in all binders was ettringite (17.9–22.4 wt%), while the amorphous content was variable (ranging from 49.1 to 71.8 wt%), and was reduced when PG was

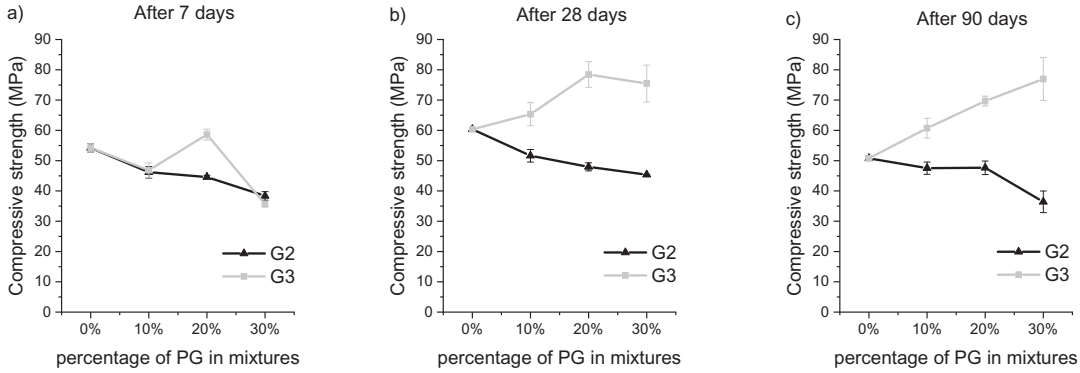

Fig. 9. Compressive strength (1σ error) of mixtures incorporating G2 and G3 after a) 7, b) 28 and c) 90 days of curing.

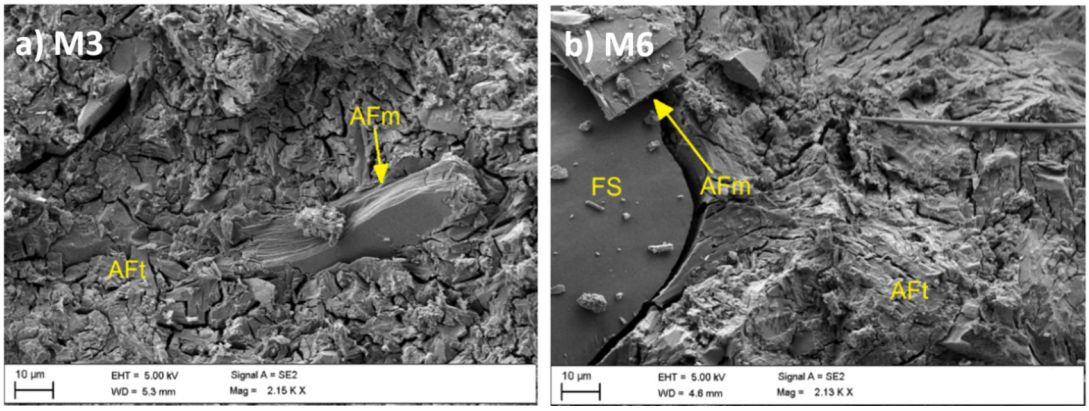

Fig. 10. SEM images of a) M3 and b) M6 after 28 days of curing.

incorporated, irrespective of its origin. The use of Finnish PG increased the monosulfate content and encouraged the formation of secondary gypsum, while it lowered the C-(A)-S-H content compared to the reference LSG. Upon using Polish PG, the aluminium-hydroxide content was diminished, while the monosulfate content was similar to the reference LSG, and the C-(A)-S-H content was equal or potentially even increased. The substitution of gypsum by Finnish PG reduced the compressive strength by 30% after 90 days of curing, compared with the reference LSG. However, when pure gypsum was replaced by Polish PG, the compressive strength increased by 60% after 90 days. This investigation revealed that the combination of LS and PG can effectively produce an almost entirely by-product-based binder.

Declarations of interest

None.

Acknowledgements

This work was supported by the Fund for Scientific Research Flanders (FWO). The authors would like to acknowledge the networking support of the COST Action TU1301, www.norm4building.org. At the University of Oulu, this work was done as part of the FLOW Project (project number 8904/31/2017) funded by Business Finland in the ERA-MIN 2 Innovation program (EU Horizon 2020 program). SSAB Europe Oy and Yara Oy are acknowledged for providing ladle slag and Finnish phosphogypsum, respectively.

References

Abdel Rahman, R.O., Zin El Abidin, D.H.A., Abou-Shady, H., 2013. Assessment of strontium immobilization in cement-bentonite matrices. Chem. Eng. J. 228, 772–780. https://doi.org/10.1016/j.cej.2013.05.034.

Akin Altun, I., Sert, Y., 2004. Utilization of weathered phosphogypsum as set retarder in Portland cement. Cement Concr. Res. 34, 677–680. https://doi.org/10.1016/j.cemconres.2003.10.017.

Al-Hwaiti, M.S., 2015. Assessment of the radiological impacts of treated phosphogypsum used as the main constituent of building materials in Jordan. Environ. Earth Sci. 74, 3159–3169. https://doi.org/10.1007/s12665-015-4354-2.

Allevi, S., Marchi, M., Scotti, F., Bertini, S., Cosentino, C., 2016. Hydration of calcium sulphoaluminate clinker with additions of different calcium sulphate sources. Mater. Struct. 49, 453–466. https://doi.org/10.1617/s11527-014-0510-5.

ASTM International, 2017. ASTM C204-17. Standard Test Methods for Fineness of Hydraulic Cement by Air-Permeability Apparatus.

Baquerizo, L.G., Matschei, T., Scrivener, K.L., Saeidpour, M., Wadsö, L., 2015. Hydration states of AFm cement phases. Cement Concr. Res. 73, 143–157. https://doi.org/10.1016/j.cemconres.2015.02.011.

Cánovas, C.R., Macías, F., Pérez-López, R., Basallote, M.D., Millán-Becerro, R., 2018. Valorization of wastes from the fertilizer industry: current status and future trends. J. Clean. Prod. 174, 678–690. https://doi.org/10.1016/j.jclepro.2017.10.293.

Chandara, C., Azizli, K.A.M., Ahmad, Z.A., Sakai, E., 2009. Use of waste gypsum to replace natural gypsum as set retarders in portland cement. Waste Manag. 29, 1675–1679. https://doi.org/10.1016/j.wasman.2008.11.014.

Chang, H., Huang, P.J., Hou, S.C., 1999. Application of thermo-Raman spectroscopy to study dehydration of CaSO4·2H2O and CaSO4·0.5H2O. Mater. Chem. Phys. 58, 12–19. https://doi.org/10.1016/S0254-0584(98)00239-9.

Council of the European Union, 2014. Council directive 2013/59/EURATOM, European basic safety standards (BSS) for protection against ionising radiation. Off. J. Eur. Union L 13/1.

European Committee for Standardization, 2016. EN 196-1. Methods of Testing Cement - Part 1: Determination of Strength.

European Committee for Standardization, 2012. EN 450-1: Fly Ash for Concrete - Part 1: Definition, Specifications and Conformity Criteria.

European Committee for Standardization, 2010. EN 196-6. Methods of Testing Cement - Part 6: Determination of Fineness.

Gastaldi, D., Paul, G., Marchese, L., Irico, S., Boccaleri, E., Mutke, S., Buzzi, L., Canonico, F., 2016. Hydration products in sulfoaluminate cements: evaluation of amorphous phases by XRD/solid-state NMR. Cement Concr. Res. 90, 162–173. https://doi.org/10.1016/j.cemconres.2016.05.014.

Gaviria, X., Borrachero, M.V., Payá, J., Monzó, J.M., Tobón, J.I., 2018. Mineralogical evolution of cement pastes at early ages based on thermogravimetric analysis (TG). J. Therm. Anal. Calorim. 132, 39–46. https://doi.org/10.1007/s10973-017-6905-0.

Gijbels, K., Nguyen, H., Kinnunen, P., Samyn, P., Schroeyers, W., Pontikes, Y., Schreurs, S., Illikainen, M., 2019. Radiological and leaching assessment of an ettringite-based mortar from ladle slag and phosphogypsum. Cement Concr. Res. (submitted in May 2019, currently under review).

Gomes, A.F.S., Lopez, D.L., Ladeira, A.C.Q., 2012. Characterization and assessment of chemical modifications of metal-bearing sludges arising from unsuitable disposal. J. Hazard Mater. 418–425, 199–200. https://doi.org/10.1016/j.jhazmat.2011.11.039.

Hammas-Nasri, I., Horchani-Naifer, K., Férid, M., Barca, D., 2019. Production of a rare earths concentrate after phosphogypsum treatment with dietary NaCl and Na2CO3 solutions. Miner. Eng. 132, 169–174. https://doi.org/10.1016/j.mineng.2018.12.013.

He, H., Suito, H., 2008. Immobilization of fluorine in aqueous solution by calcium aluminum ferrite and the mixture of calcium aluminate and gypsum. ISIJ Int. 42, 794–799. https://doi.org/10.2355/isijinternational.42.794.

Huang, Y., Qian, J., Liang, J., Liu, N., Li, F., Shen, Y., 2016. Characterization and calorimetric study of early-age hydration behaviors of synthetic ye'elimite doped with the impurities in phosphogypsum. J. Therm. Anal. Calorim. 123, 1545–1553. https://doi.org/10.1007/s10973-015-5009-y.

International Atomic Energy Agency (IAEA), 2013. Radiation Protection and Management of NORM Residues in the Phosphate Industry. IAEA, Vienna. Safety Reports Series No. 78. https://doi.org/10.1016/j.resourpol.2012.04.002.

International Organization for Standardization (ISO), 2009. ISO 13320:2009 - Particle Size Analysis: Laser Diffraction Methods.

Jansen, D., Stabler, C., Goetz-Neunhoeffer, F., Dittrich, S., Neubauer, J., 2011. Does Ordinary Portland Cement contain amorphous phase? A quantitative study using an external standard method. Powder Diffr. 26, 31–38. https://doi.org/10.1154/1.3549186.

Jiao, D., Shi, C., Yuan, Q., An, X., Liu, Y., Li, H., 2017. Effect of constituents on rheological properties of fresh concrete-A review. Cement Concr. Compos. 83, 146–159. https://doi.org/10.1016/j.cemconcomp.2017.07.016.

Jun, C., Xin, C., Futian, L., Lingchao, L., Bing, T., 2001. Influence of fluorite on the Ba-bearing sulphoaluminate cement. Cement Concr. Res. 31, 213–216. https://doi.org/10.1016/S0008-8846(00)00450-6.

Kim, J.M., Choi, S.M., Han, D., 2016. Improving the mechanical properties of rapid air cooled ladle furnace slag powder by gypsum. Constr. Build. Mater. 127, 93–101. https://doi.org/10.1016/j.conbuildmat.2016.09.102.

Kirchheim, A.P., Rodríguez, E.D., Myers, R.J., Gobbo, L.A., Monteiro, P.J.M., Dal Molin, D.C.C., de Souza, R.B., Cincotto, M.A., 2018. Effect of gypsum on the early hydration of cubic and Na-doped orthorhombic tricalcium aluminate. Materials 11, 1–17. https://doi.org/10.3390/ma11040568.

Koopman, C., Witkamp, G.J., 2002. Ion exchange extraction during continuous recrystallization of CaSO4 in the phosphoric acid production process: lanthanide extraction efficiency and CaSO4 particle shape. Hydrometallurgy 63, 137–147. https://doi.org/10.1016/S0304-386X(01)00219-5.

Le Saout, G., Lécolier, E., Rivereau, A., Zanni, H., 2004. Chemical structure of cement aged at normal and elevated temperatures and pressures. Cement Concr. Res. 36, 71–78. https://doi.org/10.1016/j.cemconres.2004.09.018.

Liu, B., Wang, S., Chen, Y., Gong, C., Lu, L., 2016. Effect of waste gypsum on the setting and early mechanical propertiesof belite-C2.75B1.25A3S cement. J. Therm. Anal. Calorim. 125, 75–83. https://doi.org/10.1007/s10973-016-5265-5.

Lou, W., Guan, B., Wu, Z., 2011. Dehydration behavior of FGD gypsum by simultaneous TG and DSC analysis. J. Therm. Anal. Calorim. 104, 661–669. https://doi.org/10.1007/s10973-010-1100-6.

Lutterotti, L., Matthies, S., Wenk, H.R., 1999. MAUD (Material Analysis Using Diffraction): a user friendly java program for Rietveld texture analysis and more. In: Szpunar, Jerzy A. (Ed.), Proceedings of the Twelfth International Conference on Textures of Materials/ICOTOM-12. National Research Press, Montreal, p. 1599.

Madsen, I.C., Scarlett, N.V.Y., Kern, A., 2011. Description and survey of methodologies for the determination of amorphous content via X-ray powder diffraction. Z. Krist. 226, 944–955. https://doi.org/10.1524/zkri.2011.1437.

Matschei, T., Lothenbach, B., Glasser, F.P., 2007. The AFm phase in Portland cement. Cement Concr. Res. 37, 118–130. https://doi.org/10.1016/j.cemconres.2006.10.010.

Nguyen, H., Adesanya, E., Ohenoja, K., Kriskova, L., Pontikes, Y., Kinnunen, P., Illikainen, M., 2019a. By-product based ettringite binder - a synergy between ladle slag and gypsum. Constr. Build. Mater. 197, 143–151. https://doi.org/10.1016/j.conbuildmat.2018.11.165.

Nguyen, H., Kinnunen, P., Carvelli, V., Mastali, M., Illikainen, M., 2019b. Strain hardening polypropylene fiber reinforced composite from hydrated ladle slag and gypsum. Compos. B Eng. 158, 328–338. https://doi.org/10.1016/j.compositesb.2018.09.056.

Nguyen, H., Staudacher, M., Kinnunen, P., Carvelli, V., Illikainen, M., 2019c. Multi-fiber reinforced ettringite-based composites from industrial side streams. J. Clean. Prod. 211, 1065–1077. https://doi.org/10.1016/j.jclepro.2018.11.241.

Pajares, I., De la Torre, A.G., Martinez-Raminez, S., Puertas, F., Blanco-Varela, M.-T., Aranda, M.A.G., 2002. Quantitative analysis of mineralized white Portland clinkers: the structure of Fluorellestadite. Powder Diffr. 17, 281–286. https://doi.org/10.1154/1.1505045.

Park, J.Y., Byun, H.J., Choi, W.H., Kang, W.H., 2008. Cement paste column for simultaneous removal of fluoride, phosphate, and nitrate in acidic wastewater. Chemosphere 70, 1429–1437. https://doi.org/10.1016/j.chemosphere.2007.09.012.

Pelletier-Chaignat, L., Winnefeld, F., Lothenbach, B., Le Saout, G., Müller, C.J., Famy, C., 2011. Influence of the calcium sulphate source on the hydration mechanism of Portland cement – calcium sulphoaluminate clinker – calcium sulphate binders. Cement Concr. Compos. 33, 551–561. https://doi.org/10.1016/j.cemconcomp.2011.03.005.

Peysson, S., Péra, J., Chabannet, M., 2005. Immobilization of heavy metals by calcium sulfoaluminate cement. Cement Concr. Res. 35, 2261–2270. https://doi.org/10.1016/j.cemconres.2005.03.015.

Potgieter, J.H., Potgieter, S.S., Mccrindle, R.I., Strydom, C.A., 2003. An investigation into the effect of various chemical and physical treatments of a South African phosphogypsum to render it suitable as a set retarder for cement. Cement Concr. Res. 33, 1223–1227. https://doi.org/10.1016/S0008-8846(03)00036-X.

Qoku, E., Bier, T.A., Westphal, T., 2017. Phase assemblage in ettringite-forming cement pastes: a X-ray diffraction and thermal analysis characterization. J. Build. Eng. 12, 37–50. https://doi.org/10.1016/j.jobe.2017.05.005.

Quillin, K., 2001. Performance of belite-sulfoaluminate cements. Cement Concr. Res. 31, 1341–1349. https://doi.org/10.1016/S0008-8846(01)00543-9.

Rashad, A.M., 2017. Phosphogypsum as a construction material. J. Clean. Prod. 166, 732–743. https://doi.org/10.1016/j.jclepro.2017.08.049.

Rietveld, H.M., 1969. A profile refinement method for nuclear and magnetic structures. J. Appl. Crystallogr. 2, 65–71. https://doi.org/10.1107/S0021889869006558.

Roussel, N., Lemaître, A., Flatt, R.J., Coussot, P., 2010. Steady state flow of cement suspensions: a micromechanical state of the art. Cement Concr. Res. 40, 77–84. https://doi.org/10.1016/j.cemconres.2009.08.026.

Saadaoui, E., Ghazel, N., Ben Romdhane, C., Massoudi, N., 2017. Phosphogypsum: potential uses and problems – a review. Int. J. Environ. Stud. 74, 558–567. https://doi.org/10.1080/00207233.2017.1330582.

Scholtzová, E., Kucková, L., Kožíšek, J., Tunega, D., 2015. Structural and spectroscopic characterization of ettringite mineral -combined DFT and experimental study. J. Mol. Struct. 1100, 215–224. https://doi.org/10.1016/j.molstruc.2015.06.075.

Shakhashiro, A., Sansone, U., Wershofen, H., Bollhöfer, A., Kim, C.K., Kim, C.S., Kis-Benedek, G., Korun, M., Moune, M., Lee, S.H., Tarjan, S., Al-Masri, M.S., 2011. The new IAEA reference material: IAEA-434 technologically enhanced naturally occurring radioactive materials (TENORM) in phosphogypsum. Appl. Radiat. Isot. 69, 231–236. https://doi.org/10.1016/j.apradiso.2010.09.002.

Shen, Y., Qian, J., Chai, J., Fan, Y., 2014. Calcium sulphoaluminate cements made with phosphogypsum: production issues and material properties. Cement Concr. Compos. 48, 67–74. https://doi.org/10.1016/j.cemconcomp.2014.01.009.

Silveira, B.I., Dantas, A.E.M., Blasques, J.E.M., Santos, R.K.P., 2003. Effectiveness of cement-based systems for stabilization and solidification of spent pot liner inorganic fraction. J. Hazard Mater. 98, 183–190. https://doi.org/10.1016/S0304-3894(02)00317-5.

Smadi, M.M., Haddad, R.H., Akour, A.M., 1999. Potential use of phosphogypsum in concrete. Cement Concr. Res. 29, 1419–1425. https://doi.org/10.1016/S0008-8846(99)00107-6.

Tayibi, H., Choura, M., López, F.A., Alguacil, F.J., López-Delgado, A., 2009. Environmental impact and management of phosphogypsum. J. Environ. Manag. 90, 2377–2386. https://doi.org/10.1016/j.jenvman.2009.03.007.

Trauchessec, R., Mechling, J.-M., Lecomte, A., Roux, A., Le Rolland, B., 2015. Hydration of ordinary Portland cement and calcium sulfoaluminate cement blends. Cement Concr. Compos. 56, 106–114. https://doi.org/10.1016/j.cemconcomp.2014.11.005.

Wallevik, J.E., 2009. Rheological properties of cement paste: thixotropic behavior and structural breakdown. Cement Concr. Res. 39, 14–29. https://doi.org/10.1016/j.cemconres.2008.10.001.

Winnefeld, F., Lothenbach, B., 2010. Hydration of calcium sulfoaluminate cements - experimental findings and thermodynamic modelling. Cement Concr. Res. 40, 1239–1247. https://doi.org/10.1016/j.cemconres.2009.08.014.

Yu, Q.L., Brouwers, H.J.H., 2012. Thermal properties and microstructure of gypsum board and its dehydration products: a theoretical and experimental investigation. Fire Mater. 36, 575–589. https://doi.org/10.1002/fam.1117.